JCI insight

RESEARCH ARTICLE

ERK hyperactivation in epidermal keratinocytes impairs intercellular adhesion and drives Grover disease pathology

Cory L. Simpson,[1,2] Afua Tiwaa,[1] Shivam A. Zaver,[3] Christopher J. Johnson,[1,4] Emily Y. Chu,[5] Paul W. Harms,[6,7] and Johann E. Gudjonsson[7]

[1]Department of Dermatology, and [2]Institute for Stem Cell and Regenerative Medicine, University of Washington, Seattle, Washington, USA. [3]Virginia Mason Medical Center, Seattle, Washington, USA. [4]University of Washington School of Medicine, Seattle, Washington, USA. [5]Department of Dermatology, Hospital of the University of Pennsylvania, Philadelphia, Pennsylvania, USA. [6]Department of Pathology and [7]Department of Dermatology, University of Michigan, Ann Arbor, Michigan, USA.

Grover disease is an acquired epidermal blistering disorder in which keratinocytes lose intercellular connections. While its pathologic features are well defined, its etiology remains unclear, and there is no FDA-approved therapy. Interestingly, Grover disease was a common adverse event in clinical trials for cancer using B-RAF inhibitors, but it remained unknown how B-RAF blockade compromised skin integrity. Here, we identified ERK hyperactivation as a key driver of Grover disease pathology. We leveraged a fluorescent biosensor to confirm that the B-RAF inhibitors dabrafenib and vemurafenib paradoxically activated ERK in human keratinocytes and organotypic epidermis, disrupting cell-cell junctions and weakening epithelial integrity. Consistent with clinical data showing that concomitant MEK blockade prevents Grover disease in patients receiving B-RAF inhibitors, we found that MEK inhibition suppressed ERK and rescued cohesion of B-RAF–inhibited keratinocytes. Validating these results, we demonstrated ERK hyperactivation in patient biopsies from vemurafenib-induced Grover disease and from spontaneous Grover disease, revealing a common etiology for both. Finally, in line with our recent identification of ERK hyperactivation in Darier disease, a genetic disorder with identical pathology to Grover disease, our studies uncovered that the pathogenic mechanisms of these diseases converge on ERK signaling and support MEK inhibition as a therapeutic strategy.

Authorship note: AT and SAZ contributed equally to this work.

Conflict of interest: CLS and SAZ are coinventors on a patent application by the University of Washington for use of MEK inhibitors to treat skin fragility disorders including Grover disease(U.S. Patent serial number: 18/596,363); CLS's spouse is an employee with stock options/holdings in UnitedHealth Group.

Submitted: May 13, 2024
Accepted: September 18, 2024
Published: September 26, 2024

Reference information: *JCI Insight*. 2024;9(21):e182983. https://doi.org/10.1172/jci.insight.182983.

Introduction

Grover disease (GD) is a spontaneous dermatologic disorder of unknown etiology that can cause intractable pruritus, extensive vesicular skin lesions in severe cases, and cutaneous superinfection (1–3). Since its first description in 1970 (4), the pathological features of GD are well defined: the combination of abnormal differentiation of keratinocytes (called dyskeratosis) and severing of their intercellular connections (termed acantholysis), leading to blister formation within the epidermis (5, 6). GD affects certain populations (e.g., older, male) and body sites (e.g., trunk) more often than others and occurs in periodic flares, which may be induced by external factors such as heat, sweating, or microbial imbalance (7). However, the molecular drivers that directly compromise epidermal integrity in GD and could explain its clinical features are poorly understood and, regrettably, GD has no FDA-approved therapies (8, 9).

Interestingly, the pathologic features of GD can be indistinguishable from a genetic blistering disorder called Darier disease (DD) (10, 11), suggesting they may share a pathogenic mechanism. In fact, recent sequencing of GD skin lesions found acquired mutations in *ATP2A2* (12), the gene linked to DD (13, 14). Both Grover- and Darier-like eruptions have been reported as common cutaneous toxicities of systemic therapy with B-RAF inhibitors, including dabrafenib and vemurafenib (15, 16), which are utilized in the treatment of *BRAF* mutant cancers such as melanoma (17–20). Paradoxically, sustained B-RAF inhibition has been shown to induce activation of MEK (21, 22), which operates downstream of RAF in the mitogen-activated protein (MAP) kinase pathway, but how this signaling aberration induces the pathologic features of GD in human epidermal keratinocytes remains unknown. In recent work, we linked DD to MEK and ERK

overactivation (23), which led us to hypothesize that MEK hyperactivity might also fuel GD pathogenesis. Consistent with this, prior retrospective analysis of patients cotreated with MEK inhibitors (e.g., trametinib (Tram)), instead of B-RAF inhibitor monotherapy, failed to develop GD as a side effect (24).

Early studies of GD using histology and electron microscopy identified defects in desmosomes (6, 25), cell-cell junctions that are essential to maintain epidermal tissue integrity (26). Given numerous studies connecting the MAP kinase pathway to the stability of desmosomes (27–34), we proposed that overactivation of MEK and downstream ERK in GD could directly compromise intercellular adhesion. We modeled drug-induced GD in human keratinocytes and in 3D organotypic epidermis (35) using B-RAF inhibitors, which weakened cell-cell adhesion in an ERK-dependent manner. To validate a role for the MAP kinase pathway in GD pathogenesis, we assessed ERK activation in skin biopsies of B-RAF inhibitor–induced GD, which led us to propose MEK inhibition could also serve as a targeted therapy for spontaneous GD.

Results

Sustained B-RAF blockade paradoxically activates ERK in human epidermal keratinocytes. In patients treated chronically with systemic B-RAF inhibitors for malignancies driven by activating *BRAF* mutations, drug-induced GD is a common cutaneous toxicity (15, 16). This has been theorized to occur via off-target effects on bystander cells — such as keratinocytes — that have WT *BRAF*. In these cells, B-RAF inhibitors cause compensatory upregulation of C-RAF, which leads to paradoxical activation of the MAP kinase pathway via downstream kinases MEK and ERK; this was originally shown in human anaplastic carcinoma cells (21). We treated normal human epidermal keratinocytes (NHEKs), the cells that manifest GD pathology, with either of the 2 B-RAF inhibitors most often reported to induce GD, dabrafenib (Dab), and vemurafenib (Vem). Treatment of keratinocytes with either B-RAF inhibitor was sufficient to increase the active phosphorylated form of ERK (pERK) compared with the drug vehicle (DMSO) as quantified by Western blotting (WB) of NHEK lysates; ERK activation was dampened by using trametinib to inhibit MEK, the upstream kinase in the MAP kinase pathway (Figure 1, A and B).

We substantiated these findings in live NHEKs using a fluorescent biosensor engineered to shuttle out of or into the nucleus upon ERK activation or inactivation, respectively (36). In live NHEKs transduced with the ERK kinase translocation reporter linked to a green fluorescent protein (ERK-KTR-Clover), we found that treatment with dabrafenib or vemurafenib induced ERK activation in a manner that could be reversed by inhibiting MEK (Figure 1, C–E). These findings confirm that NHEKs exhibit paradoxical activation of ERK upon sustained treatment with selective B-RAF inhibitors previously linked to GD in clinical studies (15, 16).

B-RAF inhibition disrupts desmosomal protein localization in epidermal keratinocytes. ERK is well known to regulate cell-cell adhesion and differentiation of keratinocytes (29, 31, 37, 38), but this MAP kinase has not been directly linked to GD pathogenesis. To test if B-RAF inhibitor–induced ERK activation impaired intercellular adhesion, we assessed the level and localization of cell-cell junction proteins in NHEKs. Compared with control keratinocytes treated with DMSO, the B-RAF inhibitors dabrafenib or vemurafenib did not appreciably alter protein levels of classical cadherins, desmosomal cadherins (DSG1, DSG2, DSG3), or their catenin-binding partner plakoglobin (PG) (Figure 2A). However, using immunofluorescence (ImF) microscopy, we found both dabrafenib and vemurafenib induced mislocalization of desmosomal proteins (Figure 2B). Compared with DMSO, NHEKs treated with B-RAF inhibitors displayed a larger amount of DSG3 and PG in the cytoplasm rather than concentrated at intercellular borders, where they are needed to anchor keratin filaments and mediate strong adhesion between neighboring keratinocytes. This was reflected in line scans across images of PG; peaks reflecting high concentration of the desmosomal protein at intercellular borders were markedly diminished in vemurafenib- or dabrafenib-treated cells (Figure 2, C and D).

Using a mechanical dissociation assay validated for measuring intercellular adhesive strength via desmosomes in keratinocyte sheets (39), we demonstrated that the disruption of desmosomal organization noted in B-RAF–inhibited NHEKs translated into marked weakening of intercellular adhesion. NHEK monolayers treated with either dabrafenib or vemurafenib exhibited a significant increase in the number of fragments generated upon mechanical stress, reflecting reduced intercellular adhesive strength (Figure 3, A and B). Together, these results indicate that B-RAF inhibitors can induce GD pathology through impaired localization of adhesive proteins, which weakens desmosomes to cause the severing of cell-cell junctions (acantholysis) in epidermal keratinocytes seen in GD biopsies, which manifests clinically as skin erosions and crusting.

MEK suppression reverses B-RAF inhibitor–induced weakening of intercellular adhesion. Given that cotreatment of patients with MEK inhibitors prevented B-RAF inhibitor–induced GD in retrospective clinical

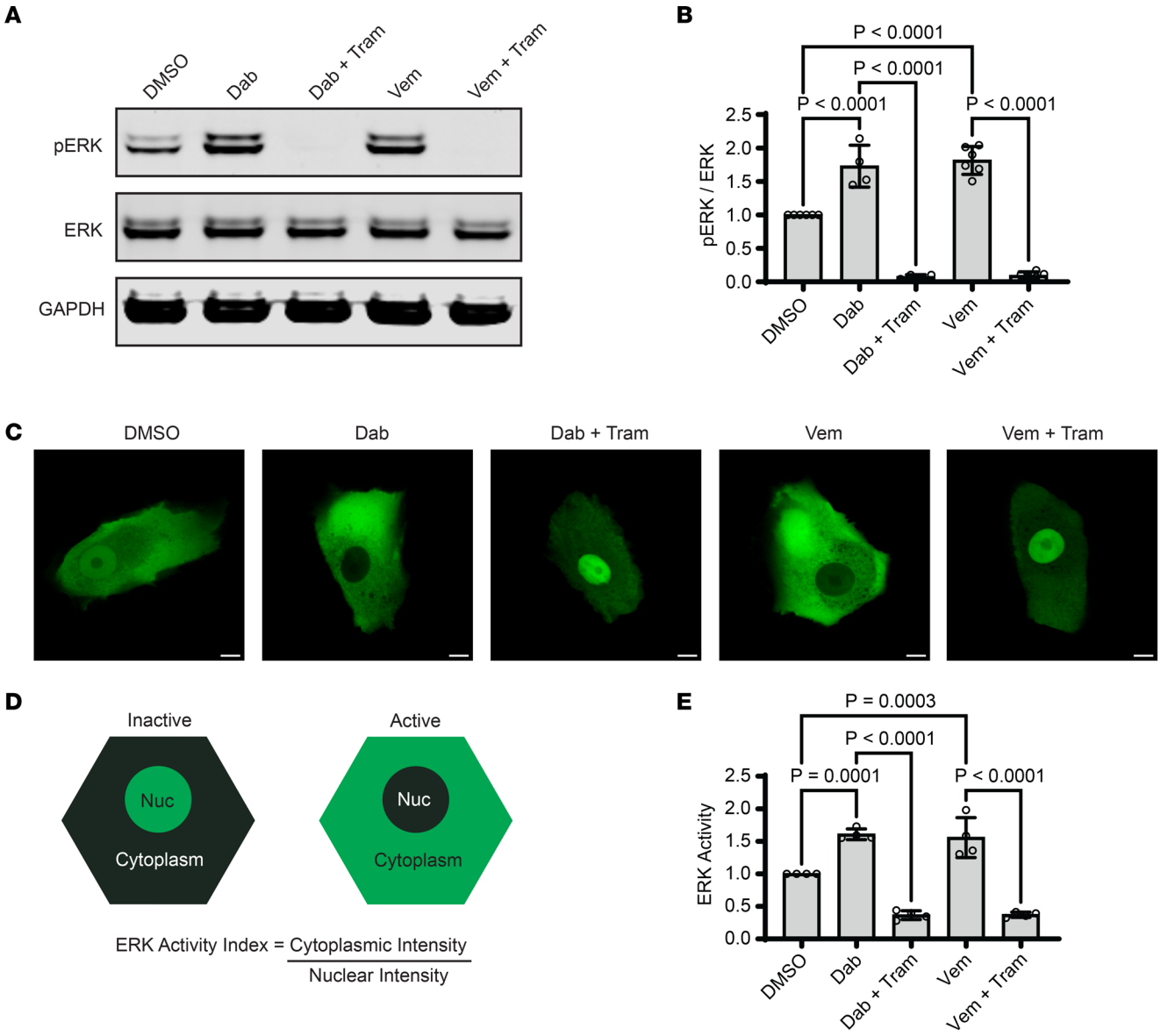

Figure 1. Sustained B-RAF blockade paradoxically activates ERK in human epidermal keratinocytes. (**A**) Immunoblot of total and phosphorylated ERK (pERK) in lysates from NHEKs treated with dabrafenib (Dab, 1 μM) or vemurafenib (Vem, 10 μM) ± trametinib (Tram, 1 μM) for 24 hours; GAPDH is a loading control. (**B**) Bar graph displays the mean ± SD of the intensity of pERK (normalized to total ERK) with individual data points plotted for $n = 4$ (Dab) or $n = 6$ (Vem) independent experiments. (**C**) Representative confocal fluorescence microscopy images of NHEKs transduced with the ERK biosensor (ERK-KTR) linked to the green mClover fluorophore; cells were treated with the indicated compounds for 24 hours in medium containing 1.2 mM calcium; Scale bar: 10 μm. (**D**) Diagram of the ERK biosensor, which is primarily localized in the nucleus when ERK is inactive versus in the cytoplasm when ERK is active; an ERK activity index is calculated as the cytoplasmic-to-nuclear fluorescence intensity ratio. (**E**) Bar graph displays the mean ± SD of ERK activity data for each treatment group with individual data points plotted for $n = 4$ biological replicates; mean ERK activity of DMSO was normalized to 1; *P* values are from 1-way ANOVA using the Bonferroni adjustment for multiple comparisons.

studies (24), we hypothesized that MEK inhibitors would rescue cell-cell junctions in dabrafenib- or vemurafenib-treated NHEKs as a model of drug-induced GD. We found trametinib, a selective MEK inhibitor FDA-approved for *BRAF* mutant cancers (18, 40), greatly enhanced the localization of desmosomal proteins to cell-cell junctions in NHEKs despite treatment with dabrafenib or vemurafenib (Figure 2, B–D).

Importantly, this rescue of cell-cell junctions in NHEKs translated into increased intercellular adhesive strength. While NHEK monolayers readily fragmented upon exposure to dabrafenib or vemurafenib, cotreatment with trametinib overcame the effect of B-RAF inhibitors, restoring the integrity of keratinocyte sheets to the level of control cultures treated with drug vehicle (Figure 3, A and B). Confirming the specificity of our findings, we tested 3 additional MEK inhibitors (U0126, PD98059, and cobimetinib), which comparably rescued cell

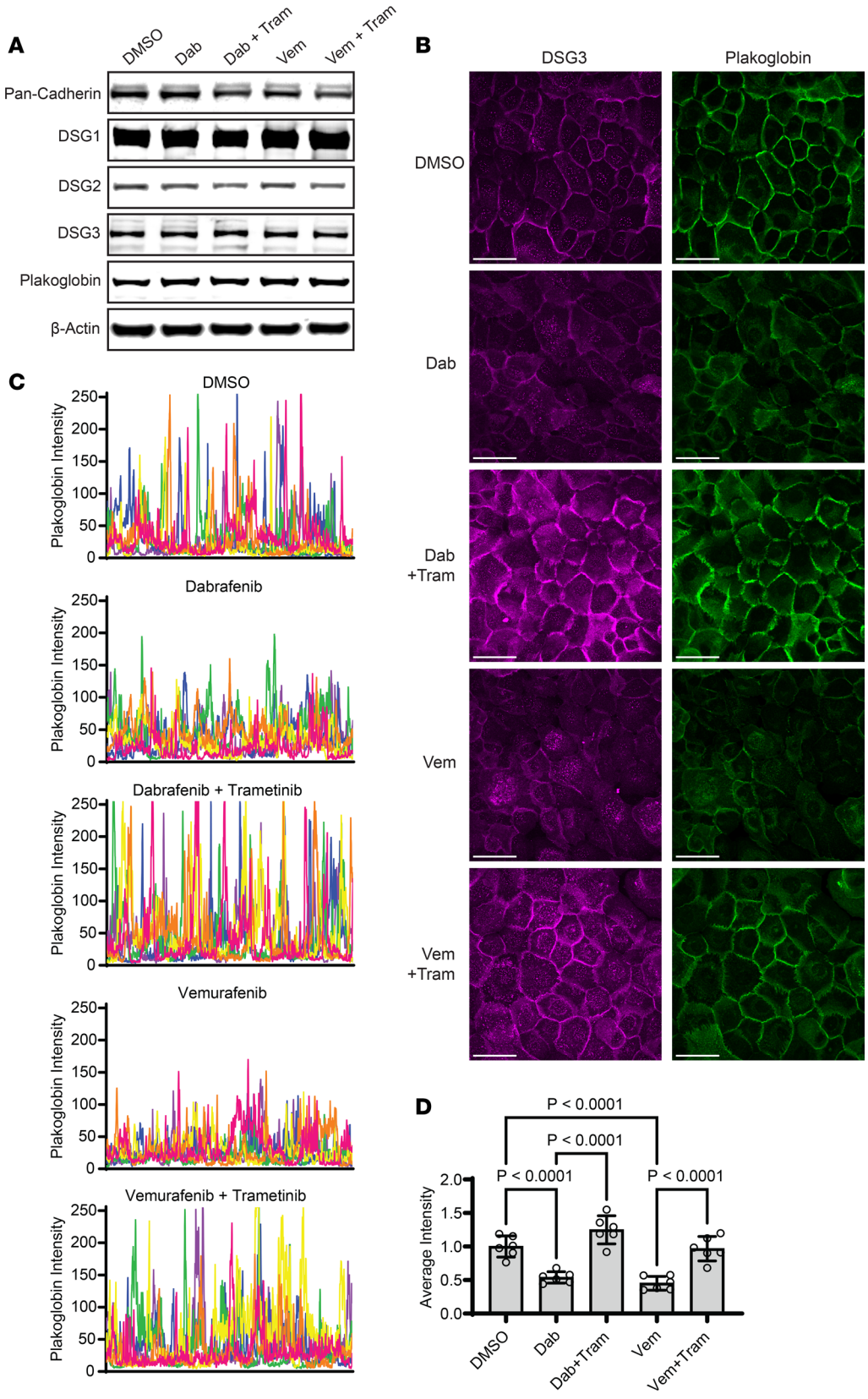

Figure 2. B-RAF inhibition disrupts desmosomal protein localization in epidermal keratinocytes. (**A**) Immunoblot of classical cadherins (Pan-Cad), desmosomal cadherins (DSG1, DSG2, DSG3), and plakoglobin (PG) in lysates from NHEKs treated with dabrafenib (Dab) or Vemurafenib (Vem) ± Trametinib (Tram) for 24 hours; β-actin is a loading control. (**B**) Confocal immunofluorescence images of DSG3 (magenta) and PG (green) in NHEKs treated with the indicated compounds for 24 hours; Scale bar: 50 μm. (**C**) Line scans were performed in a blinded manner across the entire field of 6 confocal microscopy images (individually colored pink, orange, yellow, green, blue, or purple) for each drug condition; graphs depict PG fluorescence intensity of each pixel across the entire field of view with the largest peaks occurring as the line scan crosses properly formed cell-cell junctions. (**D**) Bar graph displays the mean ± SD of the net intensity of PG with individual data points representing the average intensity across *n* = 6 independent line scans from 3 biological replicates; mean intensity for DMSO was normalized to 1; *P* values are from 1-way ANOVA using the Bonferroni adjustment for multiple comparisons.

cohesion in NHEK monolayers treated with a B-RAF inhibitor (Figure 3C and Supplemental Figure 1; supplemental material available online with this article; https://doi.org/10.1172/jci.insight.182983DS1). In contrast, blocking other MAP kinases did not rescue intercellular adhesion in B-RAF–inhibited keratinocytes; p38

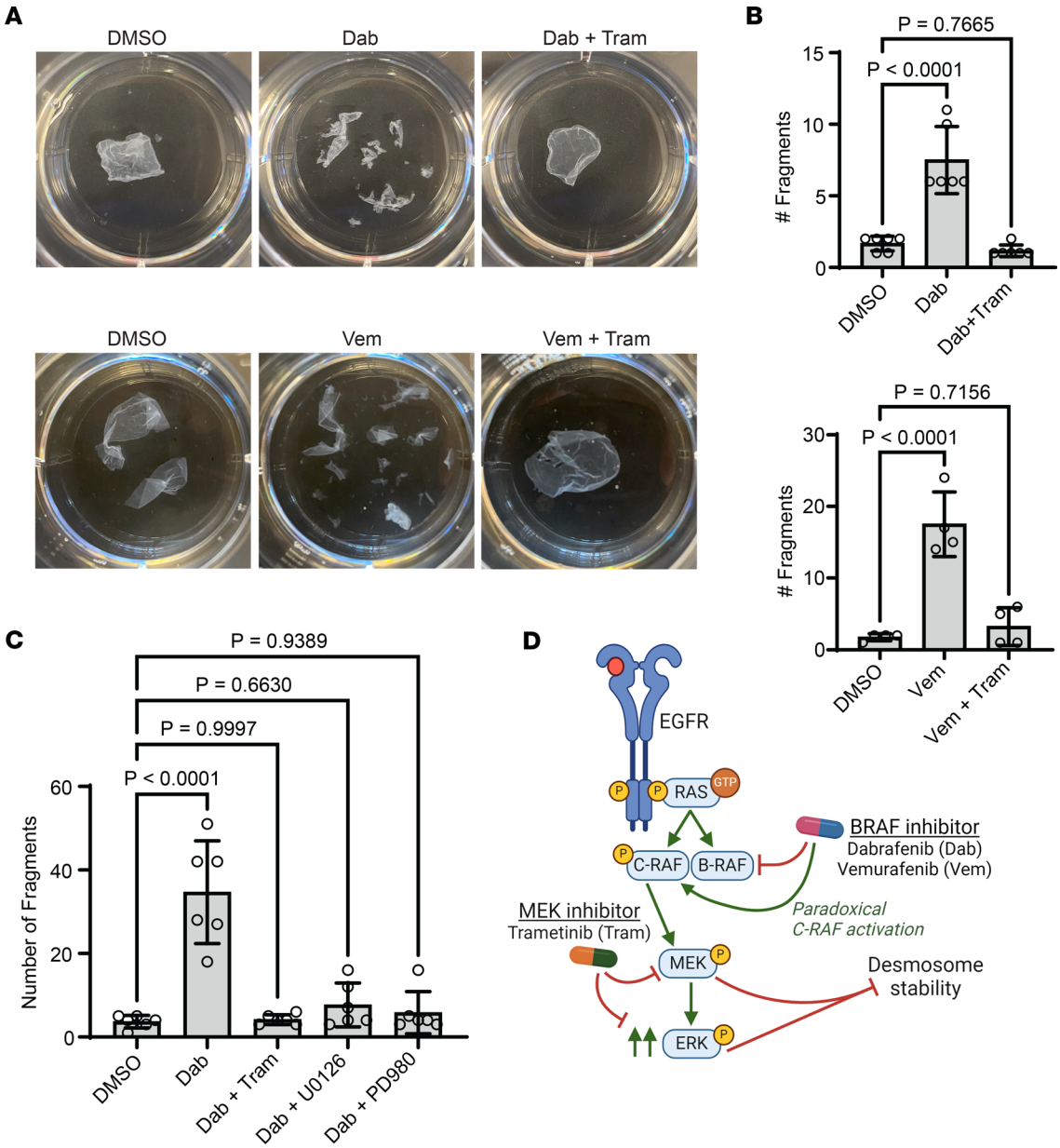

Figure 3. MEK suppression reverses B-RAF inhibitor–induced weakening of intercellular adhesion. (**A**) Mechanical dissociation assay of confluent monolayers from NHEKs cultured with the indicated compounds for 24 hours; representative images of fragmented monolayers transferred into 6-well cell culture plates are shown. (**B**) Bar graphs display the mean ± SD of the number of fragments from drug-treated monolayers with individual data points plotted for $n = 6$ (Dab) or $n = 4$ (Vem) biological replicates; P values from 1-way ANOVA with Dunnett adjustment for multiple comparisons to control cells. (**C**) Bar graph displays the mean ± SD of the number of fragments from drug-treated monolayers with individual data points plotted for $n = 6$ biological replicates; P values are from 1-way ANOVA with Dunnett adjustment for multiple comparisons to control cells. (**D**) Diagram depicts desmosome destabilization by MAP kinase pathway dysregulation; B-RAF inhibitors (e.g., dabrafenib, vemurafenib) paradoxically activate C-RAF along with MEK and ERK downstream, which inhibits desmosome stability to cause GD pathology, an effect overcome by MEK inhibitors (e.g., trametinib).

inhibition failed to restore the integrity of monolayers, while JNK inhibition actually led to an increase in fragmentation (Supplemental Figure 1). Beyond chemical inhibition of MEK, we also found that siRNA-mediated silencing of MEK expression was also able to dampen ERK activation and rescued cell-cell junctions in vemurafenib-treated keratinocytes (Supplemental Figure 2). These data further support the specificity of the therapeutic effect of dampening ERK activity to reverse B-RAF inhibitor–induced activation of MEK and resultant disruption of desmosomal adhesion in keratinocytes (Figure 3D).

B-RAF inhibitors reversibly disrupt cell-cell junctions in organotypic human epidermis. To test the effects of B-RAF inhibitors in a 3-D human tissue context, we grew NHEKs as organotypic epidermis, which

replicates fully differentiated epidermal morphology within a week (35), then treated mature cultures with vemurafenib for 48 hours. Similar to our ImF results showing impaired desmosome organization in B-RAF–inhibited keratinocyte monolayers (Figure 2B), immunostaining of desmosomal components in organotypic epidermis treated with vemurafenib revealed impaired localization of DSG1 and PG (Figure 4, A and B), the intensity of which was significantly diminished at cell-cell junctions (Figure 4, E and F). These data are also consistent with prior work that showed mislocalization of desmosomal proteins, including DSG1 and PG, within skin biopsies of GD (25).

Despite this marked alteration in cell-cell junction morphology, we did not find areas of complete acantholysis in vemurafenib-treated tissue sections, which is likely due to reduced shear mechanical forces on desmosomes within the in vitro tissue model compared with epidermis in vivo. Consistent with this, our mechanical dissociation assay required the application of shear stress to sever weakened intercellular adhesions and induce fragmentation of vemurafenib-treated keratinocyte monolayers (Figure 3, A and B). Similar to our results showing increased ERK activation by vemurafenib in keratinocyte monolayers (Figure 1), immunostaining of tissue sections from vemurafenib-treated epidermal cultures revealed a significant increase in pERK levels (Figure 4, C and D). This led us to investigate whether vemurafenib treatment induced ERK activation in patients who developed GD as a side effect of therapy.

Biopsies of B-RAF inhibitor–induced GD show ERK hyperactivation. Since GD is not a genetic disorder that can be easily replicated using knockout cells or mice, we established a model of drug-induced GD using B-RAF inhibitors that have been robustly linked in clinical studies to inducing specific GD pathology in patients (15, 16). To validate the findings from our in vitro model of drug-induced GD, we aimed to assess ERK activation levels in skin biopsies from patients treated with B-RAF inhibitor monotherapy. We obtained fixed tissue sections of skin biopsies from a deidentified cohort of 5 patients treated with vemurafenib who developed a cutaneous eruption with pathologic features diagnosed as drug-induced GD by a board-certified dermatopathologist (Figure 5A).

Immunostaining biopsies of vemurafenib-induced GD skin lesions compared with normal control skin showed disruption in the localization of both DSG1 and PG at cell-cell borders in the epidermis (Figure 5, B and C). These data are consistent with prior studies of GD (25), which demonstrated a breakdown of desmosomal adhesion within areas of keratinocyte acantholysis typical of GD lesions. Moreover, we found a significant increase in pERK levels within the epidermal lesions of vemurafenib-related GD (Figure 5, D and E, and Supplemental Figure 3). These data confirm in patients treated with vemurafenib monotherapy that B-RAF inhibition is associated with a paradoxical increase in ERK activation within skin lesions that exhibit loss of cell-cell adhesion and were diagnosed as drug-induced GD, thus directly implicating ERK signaling in GD pathogenesis. Our results explain why the addition of MEK inhibitors like trametinib, which suppress ERK overactivation, can eliminate GD as a side effect of B-RAF inhibitors.

Idiopathic GD lesions exhibit increased ERK activation. Based on our results showing that B-RAF inhibition causes overactivation of ERK in human keratinocytes, organotypic epidermis, and in patients with drug-induced GD, we proposed that this same mechanism could drive the pathology of spontaneous GD, a more common dermatologic condition that is considered idiopathic and currently lacks any FDA-approved therapy. To test this, we obtained tissue sections from 17 skin biopsies from a deidentified cohort of patients with typical pathologic features of spontaneous GD (Figure 6A) and performed immunostaining for both intercellular junctions and ERK activation.

Compared with biopsies of control skin, staining of GD biopsies revealed clear disruption of cell-cell junctions between epidermal keratinocytes. Within lesional areas, DSG1 and PG were nearly completely internalized within the cytoplasm and collapsed around the nucleus of epidermal keratinocytes rather than being localized to intercellular borders (Figure 6, B and C) Importantly, we also found a concomitant increase in ERK phosphorylation within GD lesions (Figure 6, D and E). Together, our results implicate overactivation of the MAP kinase pathway via ERK in the pathogenesis of both drug-induced and idiopathic GD and underscore the potential therapeutic value of MEK inhibitors — several of which are already cleared for clinical use — for this dermatologic disorder that is in need of new treatment strategies.

Discussion

Molecular therapies have completely changed the treatment landscape and prognosis for malignancies driven by specific mutations, such as *BRAF* V600E, in melanoma (41). Despite being highly selective for their targets, inhibitors of the MAP kinase signaling pathway have had unanticipated side effects,

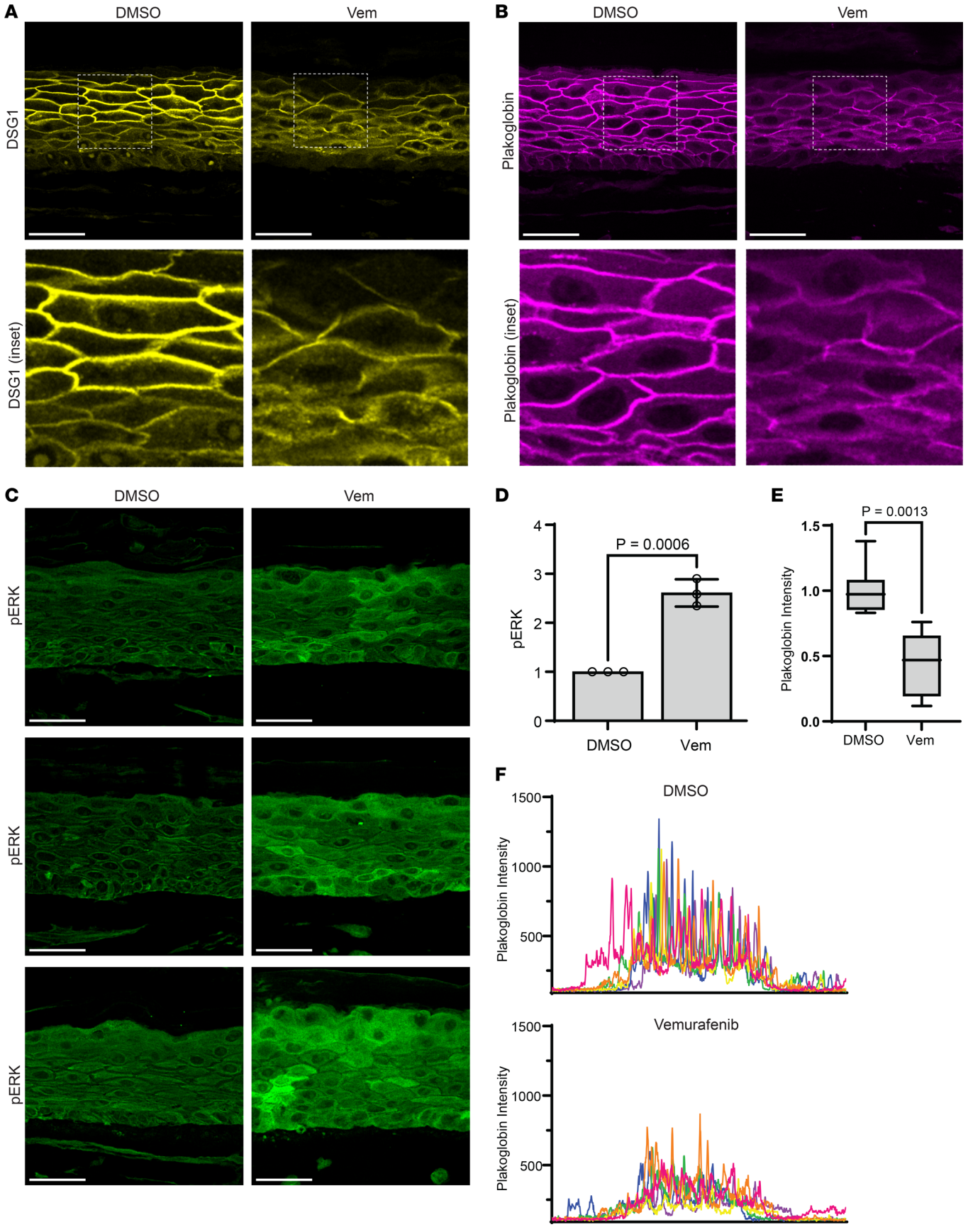

Figure 4. B-RAF inhibition is sufficient to disrupt cell-cell junctions and hyperactivate ERK in organotypic human epidermis. (**A**) Immunostaining of DSG1 (yellow) and (**B**) PG (magenta) in tissue cross sections from organotypic epidermal cultures after 48 hours of treatment with DMSO or vemurafenib (Vem),

which disrupted desmosomal protein localization to cell-cell borders; Scale bar (**A** and **B**): 50 μm; insets magnified below (original magnification, × 3). (**C**) Immunostaining of pERK (green) in tissue cross sections from epidermal cultures treated with DMSO versus vemurafenib; Scale bar: 50 μm. (**D**) Quantification of epidermal immunostaining of pERK in cross sections of DMSO- versus vemurafenib-treated cultures; bar graph displays the mean (individual values plotted) ± SD of pERK intensity from ≥ 60 images from $n = 3$ biological replicates for each drug. (**E**) Mean plakoglobin (PG) fluorescence intensity from $n = 6$ independent line scans across 3 biological replicates of DMSO-treated versus vemurafenib-treated cultures is plotted as a box plot of the 25th–75th percentile with a line at the median; mean intensity for DMSO was normalized to 1; P value from unpaired 2-tailed Student's t test. (**F**) Line scans (individually colored pink, orange, yellow, green, blue, or purple) were performed through the epidermis in 6 confocal microscopy images for each drug condition; graphs depict PG fluorescence intensity of each pixel across the epidermis with the largest peaks occurring at properly formed cell-cell junctions.

including frequent cutaneous adverse events that reduced drug safety and tolerability, impaired quality of life, and even disqualified patients from trials (42, 43). As a silver lining, off-target effects of a drug can provide insight into the pathogenesis of other diseases. In clinical trials of B-RAF–inhibitor monotherapy for cancer, investigators reported an unexpectedly common skin eruption with biopsy features diagnostic of GD (15, 16); subsequent analysis indicated GD was seen in 42.9% and 38.9% of patients treated with dabrafenib or vemurafenib, respectively (24). However, it was unclear how B-RAF blockade replicated the specific pathologic findings of a rare skin blistering disorder that had not previously been linked to this signaling pathway. We used multiple in vitro assays to demonstrate that B-RAF inhibitors are sufficient to increase ERK activation, which disrupted desmosomal adhesion in human keratinocytes and organotypic epidermis, thus explaining the loss of tissue integrity typical of GD pathology.

Intriguingly, the pathologic features of GD can be identical to DD (10, 11, 25), a genetic disorder linked to mutation of a calcium ATPase (SERCA2) embedded in the endoplasmic reticulum (12). Up to now, it remained unclear why these 2 disorders would exhibit such similar findings in biopsies that pathologists cannot consistently distinguish the diagnoses without additional clinical information, such as whether the eruption is known to be hereditary (DD) or spontaneous (GD). Our recent work established an in vitro model of DD and demonstrated that deficiency or chemical inhibition of SERCA2 induced hyperactivation of ERK (23), which we report here to also be a driver of GD pathology. Further linking these disorders with distinct origins (inherited versus acquired), some cases of GD were recently found to harbor acquired mutations in the DD–linked gene *ATP2A2* encoding SERCA2, a major regulator of calcium, which can activate ERK signaling in keratinocytes (44). The convergence of these 2 disorders upon the same signaling pathway explains the similarity of their pathologic features. Moreover, recent RNA sequencing of skin biopsies from patients with GD or DD identified an overlapping transcriptional signature that pointed to dysregulation of serum response factor and the actin cytoskeleton (45), both of which are modulated by MEK and ERK (46–48).

While molecular therapies have revolutionized the treatment of common inflammatory dermatologic conditions using monoclonal antibodies against cytokines or selective kinase inhibitors (49–52), targeted therapeutics remain elusive for rare blistering disorders. Current therapy of GD is based on case series and expert opinion as it lacks any treatment proven in prospective trials (8, 9, 53). Retinoids, which regulate the differentiation of keratinocytes, have been used in observational studies for GD (8, 9, 54–56), but they confer a high risk of toxicity with long-term use and are potent teratogens (57, 58). Other conventional but off-label therapies for GD include topical corticosteroids and repeated narrow-band ultraviolet light treatment, which is burdensome for patients (8, 9). More recently, dupilumab has been reported as an off-label treatment for refractory GD (59–61), though its blockade of IL-4 and -13 receptors may target secondary pruritus and inflammation rather than the primary pathogenic drivers of GD. Our findings suggest that MEK inhibitors, which are FDA-approved for oral administration for multiple *BRAF*-driven cancers (18, 62–66), could be therapeutic for GD as well as DD. Moreover, MEK inhibitors can be delivered topically as shown by successful use of compounded trametinib to treat a cutaneous histiocyte proliferation driven by MAP kinase overactivation (67). Topical MEK inhibitors could obviate side effects from systemic use (24, 68, 69) and their delivery is likely to be efficient for blistering disorders like GD, given that their pathology lies in the epidermis and already compromises the cutaneous barrier.

In conclusion, our results from cellular and organotypic models identified ERK as a key driver of GD pathology and demonstrate that MEK inhibition was sufficient to restore desmosomal organization and rescue intercellular adhesion in keratinocytes with hyperactive ERK signaling. Moreover, our finding of ERK hyperactivation in skin lesions from patients with both B-RAF inhibitor–induced and idiopathic GD substantiate MAP kinase signaling modulation as a viable strategy for GD treatment. The existence of multiple FDA-approved agents targeting MEK, in particular, further supports their feasibility for clinical trials for GD. While the therapeutic potential of MEK inhibitors for GD in patients has not yet been tested, data

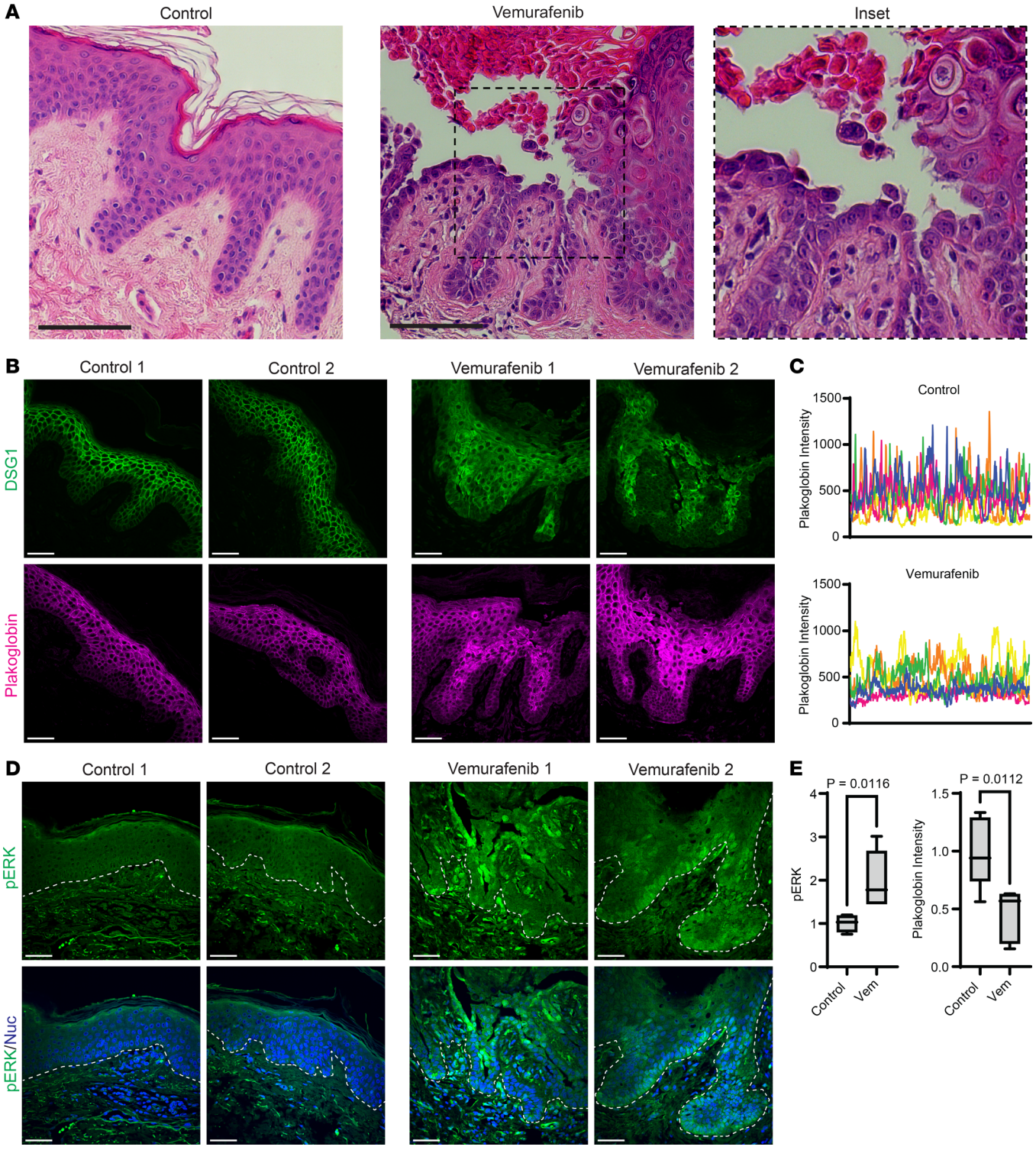

Figure 5. Biopsies of B-RAF inhibitor–induced GD show epidermal hyperactivation of ERK and disruption of desmosomal proteins. (**A**) H&E-stained cross sections of punch biopsies from the skin of an individual who was a control donor versus a patient diagnosed with vemurafenib-induced GD, which demonstrates aberrant cornification (dyskeratosis) and epidermal splitting between keratinocytes (magnified in inset [original magnification, × 2]); Scale bar: 100 μm. (**B**) Immunostaining of DSG1 (green) and plakoglobin (magenta) in tissue cross sections from patient biopsies; images shown are from 2 control donors and 2 patients with drug-induced GD and are representative of *n* = 5 patients in each group; Scale bar: 50 μm. (**C**) Line scans (individually colored pink, orange, yellow, green, or blue) were performed through the epidermis in *n* = 5 patient biopsies each for control or vemurafenib-induced GD; graphs depict plakoglobin fluorescence intensity of each pixel across the epidermis with the largest peaks occurring at properly formed cell-cell junctions. (**D**) Immunostaining of pERK (green) and Hoechst (blue) to stain nuclei (Nuc) in tissue cross-sections from patient biopsies; images shown are from 2 control donors and 2 patients with vemurafenib-induced GD and are representative of *n* = 5 patients in each group; dashed line marks bottom of the epidermis; Scale bar: 50 μm. (**E**) Quantification of epidermal immunostaining of pERK or mean plakoglobin line-scan

intensities from cross sections of control biopsies versus in lesions of vemurafenib-induced GD; pERK and plakoglobin intensity data for each group are depicted as a box plot of the 25th–75th percentile with a line at the median from n = 5 control versus n = 5 disease biopsies; control mean normalized to 1; P value from unpaired 2-tailed Student's t test.

from multiple clinical trials revealed that adding trametinib to B-RAF inhibitors eliminated drug-induced GD (24), which provides excellent rationale for clinical studies to evaluate MEK inhibitors for treatment of idiopathic GD.

Methods

Sex as a biological variable. Our in vitro studies examined available human primary and immortalized keratinocytes from males, but our results were validated using skin biopsy specimens from both male and female patients, which showed similar findings.

Reagents. Inhibitors of MEK, including trametinib (Cat. no. 62206), U0126 (Cat. no. 9903), PD98059 (Cat. no. 9900), PD184352 (Cat. no. 12147), plus inhibitors of B-RAF, including dabrafenib (Cat. no. 91942) and vemurafenib (Cat. no. 17531), were from Cell Signaling Technology. Rabbit antibodies recognizing phospho-ERK1/2 (D13.14.4E; Cat. no. 4370), pan-cadherin (Cat. no. 4068), PG (Cat. no. 75550), and mouse anti-ERK1/2 (L34F12; Cat. no. 4696) came from Cell Signaling Technology. Rabbit anti-KRT10 (Cat. no. ab76318) came from Abcam. Mouse anti-DSG1 (Cat. no. sc-137164), anti-DSG2 (Cat. no. sc-80663), anti-DSG3 (Cat. no. sc-53487), anti-PG (Cat. no. sc-514115), anti-GAPDH (Cat. no. sc-47724), and anti-β-Actin (C4; Cat. no. sc- 47778) came from Santa Cruz Biotechnologies. Mouse anti-MEK1/2 (L38C12; Cat. no. 4694) and rabbit anti-GAPDH (D16H11; Cat. no. 5174) came from Cell Signaling Technology. Chicken anti-PG (no. 1408) was a gift from Kathleen Green (Northwestern University, Chicago, Illinois, USA). Secondary antibodies for fluorescent immunoblotting, including IRDye 800CW goat anti-rabbit IgG (Cat. no. 926-32211) and IRDye 680RD goat anti-mouse IgG (Cat. no. 926-68070), came from LI-COR Biosciences. For cell and tissue staining, fluorescent secondary antibodies came from Thermo Fisher Scientific: Goat anti-mouse IgG AlexaFluor-405 (Cat. no. A31553), AlexaFluor-488 (Cat. no. A11001), AlexaFluor-594 (Cat. no. A11005), or AlexaFluor-633 (Cat. no. A21050); goat anti-rabbit IgG AlexaFluor-405 (Cat. no. A31556), AlexaFluor-488 (Cat. no. A11008), AlexaFluor-594 (Cat. no. A11012), or AlexaFluor-633 (Cat. no. A21070). Hoechst 33342 came from Thermo Fisher Scientific (Cat. no. H1399). The ERK fluorescent biosensor (pLenti-CMV-Puro-DEST-ERK-KTR-mClover; Cat. no. 59150) was from Addgene.

Cell culture. Normal human epidermal keratinocytes (NHEKs) isolated from deidentified neonatal foreskins were cultured in Medium 154 adjusted to 0.07 mM $CaCl_2$ (Thermo Fisher Scientific Cat. no. M154CF500) plus 1× human keratinocyte growth supplement (Thermo Fisher Scientific Cat. no. S0015) and 1× gentamicin/amphotericin (Thermo Fisher Scientific Cat. no. R01510).

J2-3T3 immortalized murine fibroblasts (a gift from Kathleen Green, Northwestern University, Chicago, Illinois, USA) were cultured in complete DMEM (Thermo Fisher Scientific Cat. no. 11965092) with a final concentration of 10% FBS (Hyclone, Thermo Fisher Scientific Cat. no. SH3039603), 2 mM GlutaMAX (Thermo Fisher Scientific Cat. no. 35050061), 100 U/mL penicillin, and 100 μg/mL streptomycin.

All cell lines were grown at 37°C in 5% CO_2 within an air-jacketed, humidified incubator. Cells were cultured on sterile tissue culture–treated dishes and passaged using 0.25% Trypsin-EDTA (Thermo Fisher Scientific Cat. no. 15400054) while subconfluent.

Organotypic epidermal culture. Organotypic human epidermal "raft cultures" were grown as described (35, 70). Cultures were differentiated in E-medium, containing a 3:1 mixture of DMEM:Ham's F12 (Thermo Fisher Scientific Cat. no. 11765054) along with 10% FBS, 180 μM adenine (Sigma-Aldrich Cat. no. A2786), 0.4 μg/mL hydrocortisone (Sigma-Aldrich Cat. no. H0888), 5 μg/mL human insulin (Sigma-Aldrich Cat. no. 91077C), 0.1 nM cholera toxin (Sigma-Aldrich Cat. no. C8052), 5 μg/mL apo-transferrin (Sigma-Aldrich Cat. no. T1147), plus 1.36 ng/mL 3,3′,5-tri-iodo-L-thyronine (Sigma-Aldrich Cat. no. T6397).

J2-3T3 murine fibroblasts were suspended in collagen matrix rafts in transwells (Corning Cat. no. 353091). Per raft, 1×10^6 fibroblasts were resuspended in 10% of the final desired volume of sterile reconstitution buffer (1.1 g of $NaHCO_3$ and 2.39 g of HEPES in 50 mL 0.05 N NaOH), to which was added 10% of the final desired volume of 10× DMEM (Sigma-Aldrich Cat. no. D2429). After thoroughly mixing the cells by pipetting, high-concentration rat tail collagen I (Corning Cat. no. CB354249) was added (to a final concentration of 4 mg/mL) and the slurry was supplemented with sterile diH_2O to dilute the solution

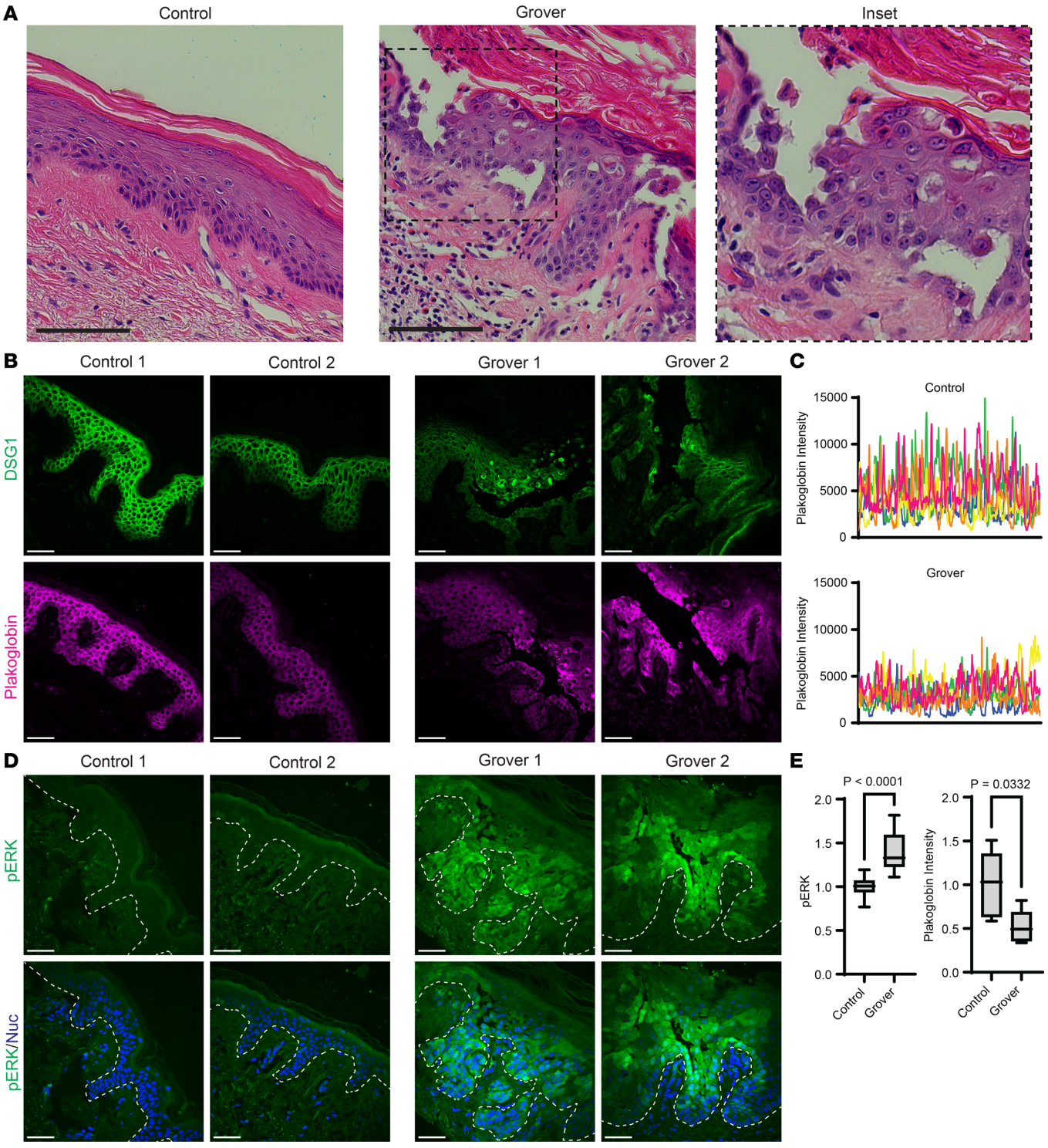

Figure 6. Idiopathic GD biopsies exhibit ERK hyperactivation along with desmosomal disruption. (**A**) H&E-stained cross sections of punch biopsies from the skin of an individual who was a control donor versus a patient with idiopathic GD, which demonstrates aberrant cornification (dyskeratosis) with retention of nuclei in the cornified layers and loss of keratinocyte cohesion (magnified in inset [original magnification, × 2]); Scale bar: 100 μm. (**B**) Immunostaining of DSG1 (green) and plakoglobin (magenta) in tissue cross-sections from patient biopsies; images shown are from 2 control donors and 2 patients with GD and are representative of n = 17 patients in each group; Scale bar: 50 μm. (**C**) Line scans (individually colored pink, orange, yellow, green, or blue) were performed through the epidermis in n = 5 patient biopsies each for control or GD; graphs depict plakoglobin fluorescence intensity of each pixel across the epidermis with the largest peaks occurring at properly formed cell-cell junctions. (**D**) Immunostaining of pERK (green) and Hoechst (blue) to stain nuclei (Nuc) in tissue cross sections from patient biopsies; images shown are from 2 control donors and 2 patients with GD and are representative of n = 17 patients in each group; dashed line marks bottom of the epidermis; Scale bar: 50 μm. (**E**) Quantification of epidermal immunostaining of pERK or mean plakoglobin line-scan intensities from cross sections of control biopsies versus in GD lesions; pERK and plakoglobin intensity data for each group are depicted as a box plot of the 25th–75th percentile with a line at the median; for pERK, n = 17 control versus n = 17 GD biopsies; for plakoglobin line-scan intensity, n = 5 control versus n = 5 GD biopsies; control mean normalized to 1; P value from unpaired 2-tailed Student's t test.

to the final desired volume, 2 mL total per raft. As needed, 0.05 N NaOH was added dropwise until the pH reached approximately 7 based on the indicator phenol red. The slurry of collagen and fibroblasts was inverted to mix, then was 2 mL was pipetted into each transwell insert suspended within a deep 6-well cell culture plate (Corning Cat. no. 08-774-183). The rafts were allowed to polymerize for 1 hour at 37°C, then were submerged in 16 mL complete DMEM and allowed to incubate overnight at 37°C.

The next day, keratinocyte cultures were trypsinized then resuspended in E-medium containing EGF (5 ng/mL) to final concentration of 0.75×10^6 cells/mL (in a final volume of 2 mL per organotypic culture). The DMEM was removed from the upper and lower transwell chambers by aspiration, then 2 mL (1.5×10^6 cells) of resuspended keratinocytes were pipetted on top of each raft. E-medium plus 5 ng/mL EGF was added to both the top and bottom transwell chambers to submerge the raft, then the cultures were incubated overnight at 37°C. After waiting 24 hours, the E-medium was removed from both the top and bottom chambers. To initiate stratification, keratinocytes were placed at an air-liquid interface by adding E-medium (lacking EGF) to only the bottom chamber until reaching the bottom of the raft. Organotypic cultures were grown for 8–12 days at 37°C with replacement of E-medium in the bottom chamber every 2 days. Chemical inhibitors or vehicle control (DMSO) were diluted in the bottom chamber E-medium. The concentration of inhibitors used were: dabrafenib (1 μM), vemurafenib (10 μM), and trametinib (1 μM). To perform histology, the entire transwell and raft culture were submerged in 10% neutral-buffered formalin (Thermo Fisher Scientific Cat. no. 22-026-435) within a 6-well cell culture plate for at least 24 hours. Organotypic epidermis was processed for histologic examination plus H&E staining by the Fred Hutchinson Cancer Center Experimental Histopathology Core.

Immunoblotting. NHEKs seeded at 1×10^6 cells per well of 6-well cell culture dishes were grown in M154 until reaching confluence, then were switched into E-medium with vehicle control (DMSO) or inhibitors as follows: Dabrafenib (1 μM), vemurafenib (10 μM), trametinib (1 μM), cobimetinib (1 μM), selumetinib (1 μM), U0126 (10 μM), PD98059 (20 μM), SB203580 (10 μM), or SP600125 (25 μM). After 24–48 hours, whole-cell lysates were made after washing cells in PBS then applying urea sample buffer [8 M Urea, 1% SDS, 10% glycerol, 0.0005% pyronin-Y, 5% β-mercaptoethanol, 60 mM Tris, pH 6.8] for 10 minutes. Lysate homogenization was performed using a microtip probe sonicator (Thermo Fisher Scientific).

Protein lysates were loaded into NuPAGE 12% Bis-Tris Gels (Thermo Fisher Scientific Cat. no. NP0343BOX) then separated by electrophoresis in NuPAGE MES SDS Running Buffer (Thermo Fisher Scientific Cat. no. NP0002). Proteins were then transferred onto Immobilon-FL membrane (Sigma-Aldrich Cat. no. IPFL85R) using transfer buffer (25 mM Tris, 192 mM glycine, 20% (v/v) methanol) for 60 minutes at 50 V. Membranes were blocked for 60 minutes at room temperature in Intercept TBS blocking buffer (LI-COR). Membranes were probed at 4°C overnight in primary antibodies in Intercept TBS blocking buffer (LI-COR). Blots were washed in 1× TBS containing 0.1% (v/v) Tween-20 (TBS-T) 3 times, then were incubated 1 hour at room temperature in Intercept TBS blocking buffer containing IRDye 800CW goat anti-rabbit IgG and/or IRDye 680RD goat anti-mouse IgG (LI-COR) at 1:10,000. Blots were washed in TBS-T 3 times, then protein bands were visualized on an Odyssey M Imaging System (LI-COR).

Fluorescent cell staining. Keratinocytes were seeded in 35 mm glass-bottom cell culture dishes (MatTek Cat. no. P35G-1.5-20-C) and grown to confluency. For staining desmosomal proteins and keratins, cells were fixed at –20°C for 2 minutes using ice-cold 100% methanol, dried, then rehydrated in PBS. For all other staining, cells were fixed using 4% paraformaldehyde at 37°C for 10 minutes. Fixed cells were then incubated for 30 minutes at 37°C in blocking buffer [0.5% (w/v) BSA(Sigma-Aldrich Cat. no. A9647), 10% (w/v) normal goat serum (NGS, Sigma-Aldrich Cat. no. G9023) in PBS]. Cells were washed once in PBS, then primary antibodies diluted in 0.5% (w/v) BSA in PBS were applied to the cells overnight at 4°C. Dilutions of primary antibodies were: mouse anti-DSG3 (1:50) and rabbit anti-PG (1:50). Cells were rinsed in PBS 3 times, then were incubated for 60 minutes at 37°C in secondary antibodies diluted 1:300 (± Hoechst at 1:500) in 0.5% (w/v) BSA in PBS. Cells were rinsed 3 times in PBS and held in PBS for confocal microscopy.

Tissue processing and histologic analysis. Formalin-fixed paraffin-embedded tissue cross-sections from human organotypic epidermis or skin biopsies underwent standard histology processing followed by hematoxylin and eosin (H&E) staining. H&E-stained tissues were imaged using a 40× long working distance, achromatic, phase-contrast objective on the EVOS FL microscope (Thermo-Fisher). H&E images were obtained on the EVOS high-sensitivity embedded interline CCD color camera.

Fluorescent tissue staining. Formalin-fixed paraffin-embedded tissue cross-sections on glass slides were baked for 2 hours at 65°C. Baked slides were immersed for 3 minutes in each of: 3 baths of

xylenes (Thermo Fisher Scientific Cat. no. X3P), 3 baths of 95% ethanol, 70% ethanol, and 3 baths of PBS. Slides were then heated to 95°C for 15 minutes in antigen retrieval buffer [0.1 M sodium citrate (pH 6.0) with 0.05% (v/v) Tween-20]. After cooling to room temperature, slides were rinsed in PBS. Tissue sections were encircled using a PAP pen hydrophobic barrier. Tissue sections were incubated in a humidified chamber for 30 minutes at 37°C in blocking buffer [0.5% (w/v) BSA, 10% (v/v) NGS in PBS]. Slides were rinsed in 3 PBS baths for 3 minutes each, then were incubated overnight at 4°C in a humidified chamber in primary antibodies diluted in 0.5% (w/v) BSA in PBS. Primary antibodies were diluted as follows: mouse anti-desmoglein 1 (1:50), mouse anti-ERK (1:400), rabbit anti-phospho-ERK (1:400), rabbit anti-cytokeratin 10 (1:3000), rabbit anti-PG (1:100), or chicken anti-PG (1:1000). Slides were then washed for 3 minutes in each of 3 baths of PBS then were incubated for 60 minutes at 37°C in a humidified chamber in secondary antibodies diluted at 1:300 (± Hoechst at 1:500) in 0.5% (w/v) BSA in PBS. Slides were washed for 3 minutes each of 3 baths of PBS. Finally, a drop of Prolong Gold (Thermo Fisher Scientific Cat. no. P36934) was applied over the tissue sections along with a no. 1.5 glass coverslip. After drying, slides were imaged using confocal microscopy.

Confocal fluorescence microscopy. A Hamamatsu ORCA-FusionBT sCMOS camera and Yokogawa W1 spinning-disk confocal (SDC) system on a Nikon Ti2 microscope were used to acquire images. Samples were illuminated with laser excitation lines (405, 488, 561, and 640 nm) and emitted fluorescence signal was captured through a 60× 1.2 NA water objective (Nikon) and standard filters.

ERK biosensor imaging. For live imaging of the ERK biosensor, NHEKs were transduced with ERK-KTR-mClover (Addgene Cat. no. 59150). HEK293FT cells were grown in complete DMEM, then transfected with 4 μg pLenti-CMV-PuroDEST-ERK-KTR-mClover DNA plus 12 μL FuGENE 6 (Promega Cat. no. E2691) in 800 μL of Opti-MEM (Thermo Fisher Scientific Cat. no. 31985070), which was added to the cells and left overnight. Lentiviral supernatants were collected the next day and polybrene (Sigma-Aldrich Cat. no. H9268) was added (4 μg/mL). M154 was removed from NHEKs and replaced with viral medium for 1 hour at 37°C. After washing in PBS, M154 was replaced and cells were expanded in culture.

ERK-KTR-mClover–transduced cells were seeded into 35 mm glass-bottom dishes in low-calcium medium (0.31 mM) and grown to confluency. Cells were then exposed to high-calcium (1.3 mM) for 24 hours, then imaged by SDC microscopy. Using Fiji, the nuclear region was encircled with the polygon tool and the "Measure" function was used to calculate the mean fluorescence intensity; after using the "Cut" function to remove the nuclear region, then remaining cytoplasmic region was encircled with the polygon tool and the "Measure" function was used to calculate the mean fluorescence intensity. The ERK activity index was calculated as the ratio of the cytoplasmic integrated fluorescence intensity (active) to the nuclear integrated fluorescence intensity.

Fluorescent immunostaining quantification. Images of immunostained cell sheets or tissue sections were obtained using SDC microscopy as above and were quantified using Fiji. Fluorescence intensity was measured on nonvisibly-labeled images of immunostained cells or tissues. The mean fluorescence intensity across the entire visual filed (for confluent cell sheets) or the epidermis (circumscribed using the "Polygon" tool), was determined using the "Measure" function to calculate the mean fluorescence intensity for each laser channel across the entire visual field of confluent cells or within the encircled epidermis. The fluorescence intensity mean from each image was averaged across all nonoverlapping high-powered fields (hpf) from multiple experimental replicates for statistical comparison; the mean intensity of pooled control samples was normalized to 1.

Line-scan fluorescence intensity measurements. Images of keratinocytes or tissue sections stained with fluorescent antibodies were quantified using line scans to assess the distribution of desmosomal proteins. A horizontal line through the entire visual field (for confluent cell sheets) or through the epidermis (for tissue sections) was drawn using the "Straight Line" function in Fiji for multiple images from each experimental condition. The "ROI Manager" was used to add the line as a region of interest and the "Multi Plot" function was used to record the fluorescence intensity at each pixel along the line in each image. The background intensity was subtracted from each intensity measurement and the average of the resulting positive values was calculated across multiple experimental replicates and compared by statistical testing. The mean intensity of pooled control samples was normalized to 1. Graphs were generated in Prism by plotting the fluorescence intensity values (y-axis) at each pixel along each line scan (x-axis) with the data from each independent image indicated by distinct colors.

RNAi-based gene silencing. Keratinocytes were seeded at 50% confluency in 35 mm plates, then were transfected with 25 nmol of AllStars Negative Control siRNA (Qiagen Cat. no. 1027280) or 25 nmol total siRNA targeting MEK1 (Qiagen Cat. no. 1027417; ID no. SI00300699) plus MEK2 (Qiagen Cat. no. 1027417; ID no. SI02225090). For each 35 mm dish, 25 nmol of siRNA was diluted in 125 μL Opti-MEM and 7.5 μl FuGENE SI Transfection Reagent (Cat. no. SI-1000) was separately diluted in 125 μL Opti-MEM. The diluted siRNA and FuGENE SI Transfection Reagent were combined and allowed to incubate for 5 minutes at room temperature, then 250 μL of the mixture was added to each 35 mm dish and incubated overnight at 37°C. At 48 hours after transfection, keratinocytes were treated with 1.2 mM calcium KSFM plus 1:1,000 dilution of DMSO or vemurafenib (10 μM) for 24 hours, then cells were fixed in methanol for immunostaining or lysed for immunoblotting as described above.

Monolayer mechanical dissociation assay. A mechanical dissociation assay was performed as described (71). Keratinocytes plated at 1×10^6 cells per well of 6-well cell culture dishes were grown to confluence, then were switched into E-medium. Vehicle control (DMSO) was compared with chemical inhibitors used at the following concentrations: Dabrafenib (1 μM), vemurafenib (10 μM), trametinib (1 μM), U0126 (10 μM), PD98059 (20 μM), cobimetinib (1 μM), SP600125 (25 μM), and SB203580 (10 μM). After 24 hours, treated monolayers were washed in PBS then incubated in 500 μL dispase (5 U/ml) in Hank's balanced salt solution (Stemcell Technologies, Cat. no. 07913) at 37°C for 30 minutes. Then, 4.5 mL PBS was added to each well and released monolayers plus all liquid were transferred into 15 mL conical tubes; all tubes were placed in a rack and inverted together up to 10 times to apply mechanical stress. Fragmented monolayers were transferred into 6-well tissue culture plates then imaged using a 12-megapixel digital camera. Fragments were counted manually in images.

Statistics. Prism version 9 (GraphPad) was used for statistical analyses and graphing. Each figure legend notes the included statistical parameters such as sample size, center definition, measures of dispersion, and statistical tests. Normality of datasets was tested using the D'Agostino-Pearson test. The means of 2 normally distributed groups were compared with a 2-tailed unpaired Student's *t* test. Means from greater than 2 normally distributed groups were compared with a 1-way ordinary ANOVA with *P* values adjusted for multiple comparisons. *P* values < 0.05 were deemed statistically significant. Each graph includes exact *P* values.

Study approval. The Penn Skin Biology and Diseases Resource-based Center (SBDRC) isolated normal human epidermal keratinocytes (NHEKs) from deidentified neonatal foreskins under a protocol (no. 808224) approved by the University of Pennsylvania Institutional Review Board (IRB). Sections of tissue from deidentified skin biopsies were procured by the SBDRC from a tissue bank under a protocol (no. 808225) approved by the University of Pennsylvania IRB. Use of deidentified tissues collected for clinical purposes, which otherwise would be discarded, was exempted for written informed consent by the IRB.

Data availability. All underlying values for graphed data are available in the Supporting Data Values file.

Author contributions

AT and SAZ were deemed to have contributed equally to the hypotheses, experimental design, and data essential to the included studies. SAZ, AT, and CLS conceptualized the project. AT, SAZ, EYC, PWH, JEG, and CLS were responsible for data curation. AT, SAZ, CJJ, and CLS were responsible for formal analysis. SAZ, AT, and CLS performed the investigation. CLS and JEG provided resources. CLS supervised the project. AT and CLS were responsible for visualization. AT, SAZ, EYC, PWH, and CLS were responsible for validation. CLS wrote the original draft of the manuscript. CLS, AT, SAZ, CJJ, EYC, PWH, and JEG reviewed and edited the manuscript.

Acknowledgments

The authors thank the Skin Biology and Diseases Resource-Based Centers at University of Pennsylvania (NIH P30-AR069589) and University of Michigan (NIH P30-AR075043) for histology services and procurement of archived biopsies and NHEKs. CLS was supported by NIH K08-AR075846, NIH R03-TR005428, and a grant from the LEO Foundation. AT was supported by NIH R03-AR082896, an Innovation Pilot Award from the University of Washington Institute for Stem Cell and Regenerative Medicine, and a grant from the Foundation for Ichthyosis and Related Skin Types. CJJ was supported by a Medical Scholars Research Fellowship from the Physician-Scientist Support Fund. PWH was supported by NIH P30-AR075043. JEG was supported by NIH P30-AR075043 and the Taubman Medical Research Institute. BioRender.com was used to make the Graphical Abstract and Figure 3D.

Address correspondence to: Cory L. Simpson, Department of Dermatology, University of Washington, 850 Republican Street D254, Seattle, Washington 98109, USA. Phone: 206.616.8350; Email: csimp99@uw.edu.

1. Wang Q, et al. Bullous Grover's disease in a Chinese Tibetan adolescent: a case report. *Clin Cosmet Investig Dermatol*. 2022;15:1371–1376.
2. Karray M, et al. Kaposi Varicelliform Eruption. In: Ackley WB, et al, eds. *StatPearls*. Treasure Island; 2022.
3. Gantz M, et al. Atypical features and systemic associations in extensive cases of Grover disease: a systematic review. *J Am Acad Dermatol*. 2017;77(5):952–957.
4. Grover RW. Transient acantholytic dermatosis. *Arch Dermatol*. 1970;101(4):426–434.
5. Weaver J, Bergfeld WF. Grover disease (transient acantholytic dermatosis). *Arch Pathol Lab Med*. 2009;133(9):1490–1494.
6. Grover RW. Transient acantholytic dermatosis. Electron microscope study. *Arch Dermatol*. 1971;104(1):26–37.
7. Harmon RM, et al. Pumping the breaks on acantholytic skin disorders: targeting calcium pumps, desmosomes, and downstream signaling in Darier, Hailey-Hailey, and Grover disease [published online August 28, 2024]. *J Invest Dermatol*. https://doi.org/10.1016/j.jid.2024.06.1289.
8. Bellinato F, et al. Clinical features and treatments of transient acantholytic dermatosis (Grover's disease): a systematic review. *J Dtsch Dermatol Ges*. 2020;18(8):826–833.
9. Aldana PC, Khachemoune A. Grover disease: review of subtypes with a focus on management options. *Int J Dermatol*. 2020;59(5):543–550.
10. See SHC, et al. Distinguishing histopathologic features of acantholytic dermatoses and the pattern of acantholytic hypergranulosis. *J Cutan Pathol*. 2019;46(1):6–15.
11. Chalet M, et al. Transient acantholytic dermatosis: a reevaluation. *Arch Dermatol*. 1977;113(4):431–435.
12. Seli D, et al. Association of somatic ATP2A2 damaging variants with Grover disease. *JAMA Dermatol*. 2023;159(7):745–749.
13. Sakuntabhai A, et al. Mutations in ATP2A2, encoding a Ca2+ pump, cause Darier disease. *Nat Genet*. 1999;21(3):271–277.
14. Jacobsen NJ, et al. ATP2A2 mutations in Darier's disease and their relationship to neuropsychiatric phenotypes. *Hum Mol Genet*. 1999;8(9):1631–1636.
15. Anforth R, et al. Cutaneous toxicities of RAF inhibitors. *Lancet Oncol*. 2013;14(1):e11–e18.
16. Chu EY, et al. Diverse cutaneous side effects associated with BRAF inhibitor therapy: a clinicopathologic study. *J Am Acad Dermatol*. 2012;67(6):1265–1272.
17. Fu L, et al. Targeting extracellular signal-regulated protein kinase 1/2 (ERK1/2) in cancer: an update on pharmacological small-molecule inhibitors. *J Med Chem*. 2022;65(20):13561–13573.
18. Flaherty KT, et al. Improved survival with MEK inhibition in BRAF-mutated melanoma. *N Engl J Med*. 2012;367(2):107–114.
19. Flaherty KT, et al. Combined BRAF and MEK inhibition in melanoma with BRAF V600 mutations. *N Engl J Med*. 2012;367(18):1694–1703.
20. Falchook GS, et al. Activity of the oral MEK inhibitor trametinib in patients with advanced melanoma: a phase 1 dose-escalation trial. *Lancet Oncol*. 2012;13(8):782–789.
21. Poulikakos PI, et al. RAF inhibitors transactivate RAF dimers and ERK signalling in cells with wild-type BRAF. *Nature*. 2010;464(7287):427–430.
22. Lacouture ME, et al. Reducing skin toxicities from EGFR inhibitors with topical BRAF inhibitor therapy. *Cancer Discov*. 2021;11(9):2158–2167.
23. Zaver SA, et al. Targeting SERCA2 in organotypic epidermis reveals MEK inhibition as a therapeutic strategy for Darier disease. *JCI Insight*. 2023;8(18):e170739.
24. Carlos G, et al. Cutaneous toxic effects of BRAF inhibitors alone and in combination with MEK inhibitors for metastatic melanoma. *JAMA Dermatol*. 2015;151(10):1103–1109.
25. Hashimoto K, et al. Desmosomal dissolution in Grover's disease, Hailey-Hailey's disease and Darier's disease. *J Cutan Pathol*. 1995;22(6):488–501.
26. Simpson CL, et al. Deconstructing the skin: cytoarchitectural determinants of epidermal morphogenesis. *Nat Rev Mol Cell Biol*. 2011;12(9):565–580.
27. Valenzuela-Iglesias A, et al. Desmoglein 1 regulates invadopodia by suppressing EGFR/Erk signaling in an Erbin-dependent manner. *Mol Cancer Res*. 2019;17(5):1195–1206.
28. Kam CY, et al. Desmoplakin maintains gap junctions by inhibiting Ras/MAPK and lysosomal degradation of connexin-43. *J Cell Biol*. 2018;217(9):3219–3235.
29. Harmon RM, et al. Desmoglein-1/Erbin interaction suppresses ERK activation to support epidermal differentiation. *J Clin Invest*. 2013;123(4):1556–1570.
30. Getsios S, et al. Desmoglein 1-dependent suppression of EGFR signaling promotes epidermal differentiation and morphogenesis. *J Cell Biol*. 2009;185(7):1243–1258.
31. Egu DT, et al. Role of PKC and ERK signaling in epidermal blistering and desmosome regulation in pemphigus. *Front Immunol*. 2019;10:2883.
32. Hutz K, et al. Loss of desmoglein 2 promotes tumorigenic behavior in pancreatic cancer cells. *Mol Carcinog*. 2017;56(8):1884–1895.
33. Wei Z, et al. Pinin facilitated proliferation and metastasis of colorectal cancer through activating EGFR/ERK signaling pathway. *Oncotarget*. 2016;7(20):29429–29439.
34. Spindler V, et al. Plakoglobin but not desmoplakin regulates keratinocyte cohesion via modulation of p38MAPK signaling. *J Invest Dermatol*. 2014;134(6):1655–1664.
35. Simpson CL, et al. RNA interference in keratinocytes and an organotypic model of human epidermis. *Methods Mol Biol*. 2010;585:127–146.
36. De la Cova C, et al. A real-time biosensor for ERK activity reveals signaling dynamics during C. elegans cell fate specification. *Dev Cell*. 2017;42(5):542–553.

37. Hiratsuka T, et al. Regulation of ERK basal and pulsatile activity control proliferation and exit from the stem cell compartment in mammalian epidermis. *Proc Natl Acad Sci U S A*. 2020;117(30):17796–17807.
38. Khavari TA, Rinn J. Ras/Erk MAPK signaling in epidermal homeostasis and neoplasia. *Cell Cycle*. 2007;6(23):2928–2931.
39. Hudson TY, et al. In vitro methods for investigating desmoplakin-intermediate filament interactions and their role in adhesive strength. *Methods Cell Biol*. 2004;78:757–786.
40. Roskoski R, Jr. Targeting ERK1/2 protein-serine/threonine kinases in human cancers. *Pharmacol Res*. 2019;142:151–168.
41. Flaherty KT. Dividing and conquering: controlling advanced melanoma by targeting oncogene-defined subsets. *Clin Exp Metastasis*. 2012;29(7):841–846.
42. Belum VR, et al. Dermatological adverse events from BRAF inhibitors: a growing problem. *Curr Oncol Rep*. 2013;15(3):249–259.
43. Mondaca S, et al. Balancing RAF, MEK, and EGFR inhibitor doses to achieve clinical responses and modulate toxicity in BRAF V600E colorectal cancer. *JCO Precis Oncol*. 2018;2018:PO.18.00088.
44. Schmidt M, et al. Ras-independent activation of the Raf/MEK/ERK pathway upon calcium-induced differentiation of keratinocytes. *J Biol Chem*. 2000;275(52):41011–41017.
45. Roth-Carter QR, et al. Transcriptional profiling of rare acantholytic disorders suggests common mechanisms of pathogenesis. *JCI Insight*. 2023;8(16):e168955.
46. Pagel JI, Deindl E. Early growth response 1--a transcription factor in the crossfire of signal transduction cascades. *Indian J Biochem Biophys*. 2011;48(4):226–235.
47. Assoian RK, Klein EA. Growth control by intracellular tension and extracellular stiffness. *Trends Cell Biol*. 2008;18(7):347–352.
48. Pullikuth AK, Catling AD. Scaffold mediated regulation of MAPK signaling and cytoskeletal dynamics: a perspective. *Cell Signal*. 2007;19(8):1621–1632.
49. Silverberg N. Emerging therapies in genodermatoses. *Clin Dermatol*. 2020;38(4):462–466.
50. Hill CR, Theos A. What's new in genetic skin diseases. *Dermatol Clin*. 2019;37(2):229–239.
51. David E, et al. The evolving landscape of biologic therapies for atopic dermatitis: Present and future perspective. *Clin Exp Allergy*. 2023;53(2):156–172.
52. Lin CP, et al. Current and emerging biologic and small molecule systemic treatment options for psoriasis and psoriatic arthritis. *Curr Opin Pharmacol*. 2022;67:102292.
53. Sousou JM, et al. Management and treatment of Grover's disease: a case report and review of literature. *Cureus*. 2022;14(4):e24082.
54. Pasmatzi E, et al. Persistent generalized Grover disease: complete remission after treatment with oral acitretin. *Dermatol Online J*. 2019;25(3):9.
55. Hrin ML, et al. Methotrexate versus acitretin for Grover's disease refractory to topical therapies. *J Cutan Med Surg*. 2023;28(1):68–69.
56. Helfman RJ. Grover's disease treated with isotretinoin. Report of four cases. *J Am Acad Dermatol*. 1985;12(6):981–984.
57. Zaenglein AL, et al. Consensus recommendations for the use of retinoids in ichthyosis and other disorders of cornification in children and adolescents. *Pediatr Dermatol*. 2021;38(1):164–180.
58. Doolan BJ, et al. Retinoid-induced skeletal hyperostosis in disorders of keratinization. *Clin Exp Dermatol*. 2022;47(12):2273–2276.
59. Shelton E, et al. Can't handle the itch? Refractory immunotherapy-related transient acantholytic dermatosis: prompt resolution with dupilumab. *JAAD Case Rep*. 2022;22:31–33.
60. Barei F, et al. A case of Grover disease treated with Dupilumab: just serendipity or a future perspective? *Dermatol Ther*. 2022;35(5):e15429.
61. Butler DC, et al. Treatment of Grover disease with Dupilumab. *JAMA Dermatol*. 2021;157(3):353–356.
62. Ram T, et al. MEK inhibitors in cancer treatment: structural insights, regulation, recent advances and future perspectives. *RSC Med Chem*. 2023;14(10):1837–1857.
63. Bouffet E, et al. Dabrafenib plus Trametinib in pediatric glioma with BRAF V600 mutations. *N Engl J Med*. 2023;389(12):1108–1120.
64. Wen PY, et al. Dabrafenib plus trametinib in patients with $BRAF^{V600E}$-mutant low-grade and high-grade glioma (ROAR): a multicentre, open-label, single-arm, phase 2, basket trial. *Lancet Oncol*. 2022;23(1):53–64.
65. Subbiah V, et al. Dabrafenib and Trametinib treatment in patients with locally advanced or metastatic BRAF V600-mutant anaplastic thyroid cancer. *J Clin Oncol*. 2018;36(1):7–13.
66. Planchard D, et al. Dabrafenib plus trametinib in patients with previously untreated $BRAF^{V600E}$-mutant metastatic non-small-cell lung cancer: an open-label, phase 2 trial. *Lancet Oncol*. 2017;18(10):1307–1316.
67. Fay CJ, et al. Treatment-refractory cutaneous Rosai-Dorfman disease responsive to oral methotrexate and topical trametinib. *JAAD Case Rep*. 2023;39:74–77.
68. Abdel-Rahman O, et al. Risk of selected dermatological toxicities in cancer patients treated with MEK inhibitors: a comparative systematic review and meta-analysis. *Future Oncol*. 2015;11(24):3307–3319.
69. Anforth R, et al. Acneiform eruptions: a common cutaneous toxicity of the MEK inhibitor trametinib. *Australas J Dermatol*. 2014;55(4):250–254.
70. Simpson CL, et al. NIX initiates mitochondrial fragmentation via DRP1 to drive epidermal differentiation. *Cell Rep*. 2021;34(5):108689.
71. Simpson CL, et al. Plakoglobin rescues adhesive defects induced by ectodomain truncation of the desmosomal cadherin desmoglein 1: implications for exfoliative toxin-mediated skin blistering. *Am J Pathol*. 2010;177(6):2921–2937.